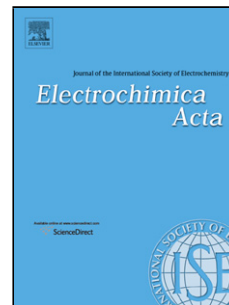


Accepted Manuscript

Title: Efficient Small Molecule Organic Dyes Containing Different Bridges in Donor Moieties for Dye-Sensitized Solar Cells

Authors: Haobin Wang, BenZhou Bao, Xiangyu Hu, Jing-Kun Fang



PII: S0013-4686(17)31730-9
DOI: <http://dx.doi.org/10.1016/j.electacta.2017.08.089>
Reference: EA 30093

To appear in: *Electrochimica Acta*

Received date: 16-7-2017
Revised date: 13-8-2017
Accepted date: 14-8-2017

Please cite this article as: Haobin Wang, BenZhou Bao, Xiangyu Hu, Jing-Kun Fang, Efficient Small Molecule Organic Dyes Containing Different Bridges in Donor Moieties for Dye-Sensitized Solar Cells, *Electrochimica Acta* <http://dx.doi.org/10.1016/j.electacta.2017.08.089>

This is a PDF file of an unedited manuscript that has been accepted for publication. As a service to our customers we are providing this early version of the manuscript. The manuscript will undergo copyediting, typesetting, and review of the resulting proof before it is published in its final form. Please note that during the production process errors may be discovered which could affect the content, and all legal disclaimers that apply to the journal pertain.

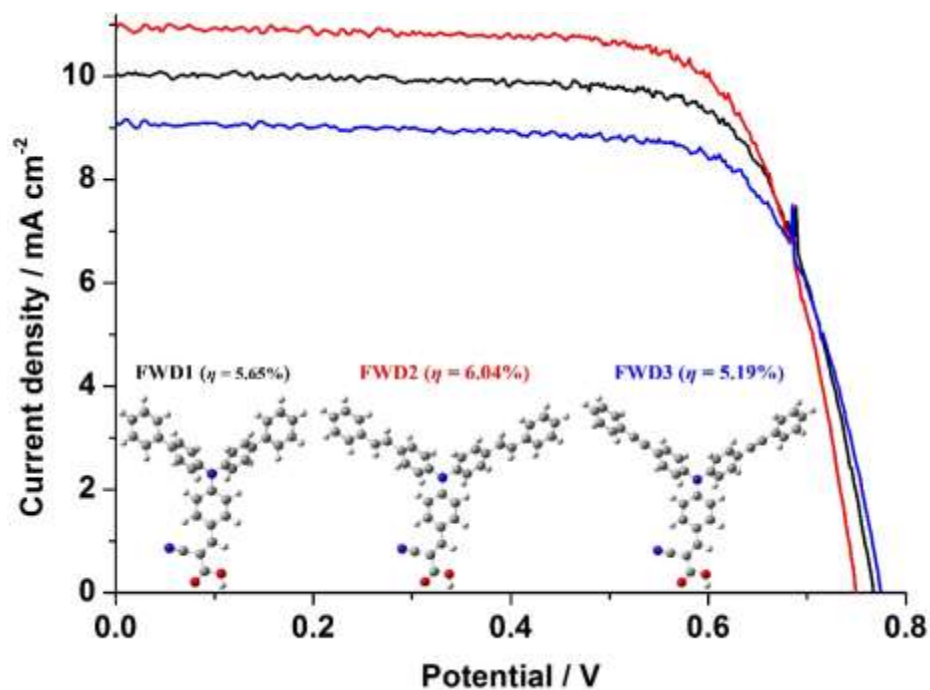
Efficient Small Molecule Organic Dyes Containing Different Bridges in Donor Moieties for Dye-Sensitized Solar Cells

Haobin Wang, BenZhou Bao, Xiangyu Hu, Jing-Kun Fang*

Department of Chemistry, School of Chemical Engineering, Nanjing University of Science and Technology, Xiaolingwei Street No. 200, Nanjing 210094, China

E-mail of corresponding author Jing-Kun Fang: fjk@njust.edu.cn

Graphical abstract



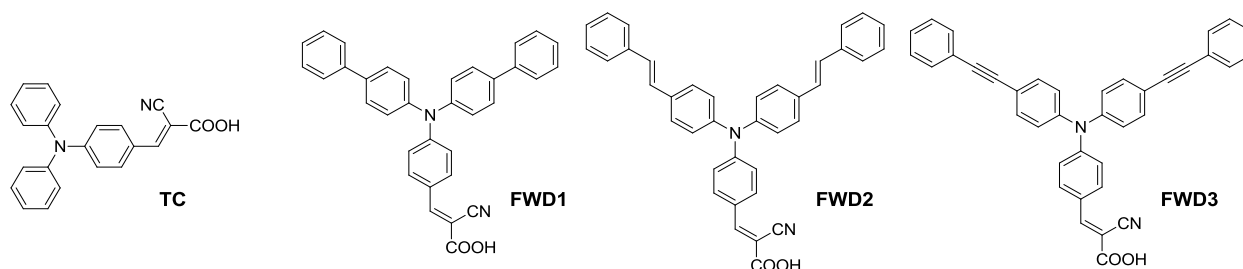
Abstract

Small molecule (molecular weight is around 500 Da) organic dyes were synthesized and used as sensitizers for the dye-sensitized solar cells (DSSCs). The optical and electrochemical properties, theoretical studies and photovoltaic parameters of DSSCs based on these dyes were systematically investigated. In order to extend the conjugation extent, two extra phenyl units were attached to triphenylamine (TPA) units bridged with single bonds, double bonds or triple bonds, respectively. The DSSCs based on **FWDS** exhibited well performances: the short-circuit current density (J_{sc}) of 10.04, 10.91 and 9.12 mA cm⁻², respectively; the open circuit voltage (V_{oc}) of 0.77, 0.75 and 0.78 V, respectively; the power conversion efficiency (η) of 5.65%, 6.04% and 5.19%, respectively. Two extra phenyl units attached via double or triple bonds increase the planar nature of these molecules, increasing the loading amount, which ultimately can correlate into the received efficiency. The results indicated that it is an effective way to get efficient dyes by introducing extra phenyl rings into donor moiety especially adopting double bonds as the bridge. Finally, efficient DSSCs were achieved by using small molecule TPA-type dyes **FWD1**, **FWD2** and **FWD3** as the sensitizers.

Keywords: Dye-sensitized solar cells; Organic dyes; Small molecule dyes; Triphenylamine; Photovoltaic performances

1 Introduction

Photosensitizers for Dye-Sensitized Solar Cells (DSSCs) have been widely developed since DSSC was firstly reported by Grätzel [1]. Even though the Ruthenium-based complex are regarded as the most efficient and successful sensitizers [2-4], issues such as containing heavy metal and high cost limit their application. Organic dyes have been extensively investigated for DSSCs for the sake of their environmental safety and low cost [5-9]. Triphenylamine (TPA) unit is widely applied in DSSCs as an excellent building block for its electron donating property and pyramidal structure [10-13]. Wielopolski and coworkers reported that the extended conjugation of TPA as a donor would make the LUMO+1 shift to lower energy levels and give a lower energy gap between LUMO and LUMO+1 resulting in wider absorption spectra [14]. Thus, many extended conjugation TPA-type dyes were developed with well light harvesting capabilities and high power conversion efficiencies [15-17]. Both single bonds and multiple bonds could be options for bridging the different conjugation units [18-20]. Due to the lack of coplanarity of the connecting parts, dye aggregation could be suppressed by adopting single-bond-bridge, which could improve the device performance efficiently [12, 21]. However, the lack of coplanarity would meanwhile limit the absorption spectra range and hence restrict the utilization of the solar energy [22, 23]. This problem can be avoided by adopting multiple-bond-bridge (double or triple bond) leading to an extended conjugation range [24, 25].

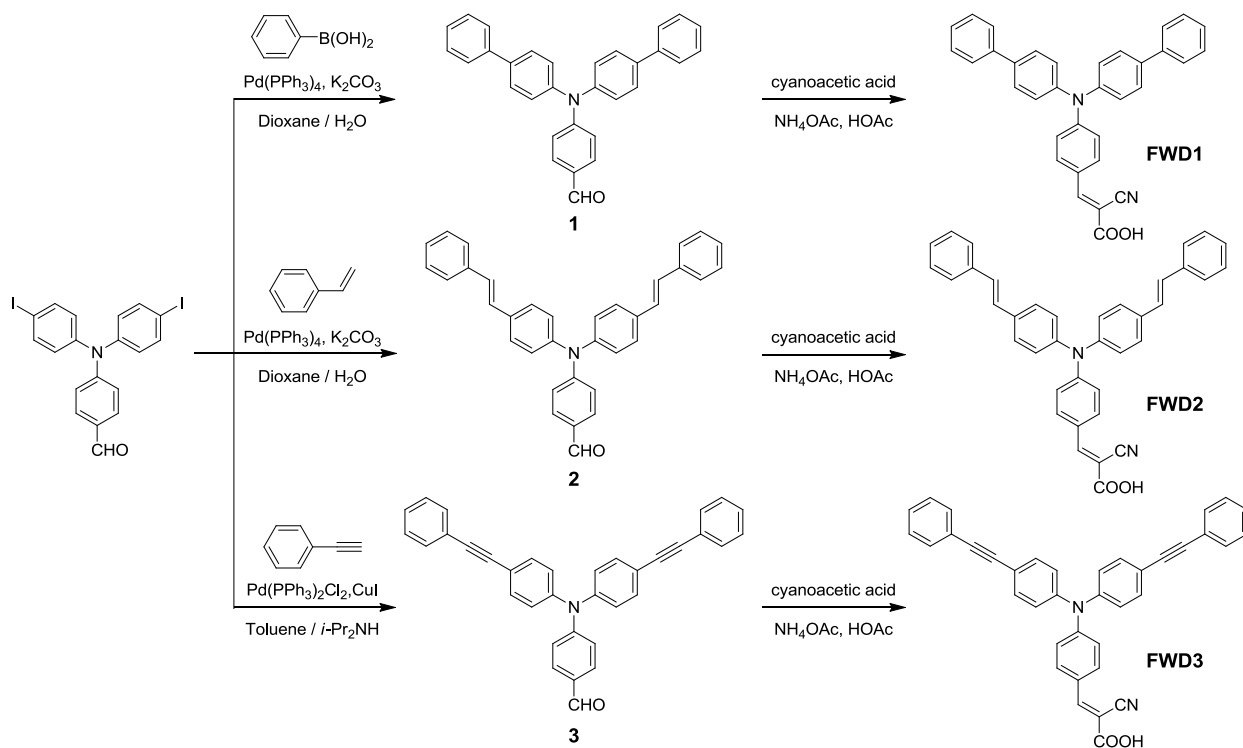


Scheme 1. Molecular structures of TPA-type dyes

2-cyano-3-(4-(diphenylamino)phenyl)acrylic acid (**TC**), as the simplest TPA-type dye, has been reported by Teng and coworkers [26]. Obviously, the scant conjugation extent of **TC** would restrict its light harvesting capability and hence low power conversion efficiency was observed (2.6%). In this work, based on dye **TC**, three conjugation extended TPA-type dyes (**FWD1**, **FWD2** and **FWD3**) were designed and synthesized by introducing two extra phenyl units to TPA units bridged with single bonds, double bonds or triple bonds, respectively (Scheme 1). The extra phenyl units were introduced into donor moiety aiming to reduce to energy gap, and we want to investigate the different effects caused by adopting different kind of bridges to the donor part. The structures of **FWDs** are shown in Scheme 1. The photophysical and electrochemical properties of **FWDs** as well as their applications in DSSCs are reported.

2 Results and discussion

2.1 Design and synthesis of dyes



Scheme 2. Synthetic routes of dyes **FWDs**.

Scheme 2 depicts the synthetic routes for **FWDs**. Intermediate **1~3** could be easily synthesized from 4-(bis(4-iodophenyl)amino)benzaldehyde as the starting material by a Suzuki reaction with phenylboronic acid, a Heck reaction with styrene or a Sonogashira reaction with phenylacetylene, respectively. Then the aldehyde **1~3** reacted with cyanoacetic acid would give the desired dyes **FWD1**, **FWD2** and **FWD3** by Knoevenagel reaction. All of the procedure gave the desired products in good yields. Dyes **FWD1**, **FWD2** and **FWD3** were fully characterized with ^1H NMR, ^{13}C NMR and HRMS, etc.

2.2 UV-Vis absorption spectra

Fig. 1. UV-Vis absorption spectra of **FWDs** in EtOH solutions (a) and adsorbed on TiO_2 films (b).

The absorption spectra of **FWDs** were measured to study their light harvesting capabilities. The UV-vis absorption spectra of **FWDs** in EtOH solutions at a concentration of 5×10^{-5} M and adsorbed on 2 μm transparent TiO_2 films are shown in Fig. 1. The corresponding data are listed in Table 1.

Table 1

Optical and electrochemical data of **FWDs**.

Dye	$\lambda_{\text{abs}}/\text{nm}^{\text{a}}$ ($\epsilon/10^4 \text{ M}^{-1} \text{ cm}^{-1}$)	$\lambda_{\text{abs}}/\text{nm}$ (TiO_2)	$E_{\text{ox}}/\text{V}^{\text{b}}$	$E_{0-0}/\text{V}^{\text{c}}$	$E_{\text{red}}/\text{V}^{\text{d}}$	μ/Debye	Band gap ^e
FWD1	410 (2.30)	414	1.30	2.46	-1.16	8.38	3.06
	332 (1.69)						
FWD2	424 (3.12)	424	1.09	2.34	-1.25	8.31	2.83
	375 (4.11)						
FWD3	410 (3.06)	413	1.35	2.48	-1.13	8.06	2.90
	355 (4.16)						

^a Measured in EtOH solution.

^b First oxidation peak potentials (E_{ox}) (vs NHE) were calibrated with ferrocene (0.63 V vs NHE).

^c E_{0-0} transition energy measured at the onset of absorption spectra.

^d $E_{\text{red}} = E_{\text{ox}} - E_{0-0}$.

^e DFT/B3LYP calculated values.

Two major strong absorption bands of **FWDs** in the visible region were observed, which can be ascribed to the localized aromatic π - π^* transition of the TPA moieties and the intramolecular charge transfer (ICT) from the donor (TPA) to the acceptor (cyanoacetic acid) with some delocalized π - π^* transition character [27]. The absorption maximum (λ_{abs}) of **FWD2** (424 and 375 nm), adopting double bonds as the bridge between the phenyl and triphenylamine units, exhibited obvious bathochromic shifts compared with that of **FWD1** (410 and 332 nm) adopting single bonds as the bridge and **FWD3** (410 and 355 nm) adopting triple bonds as the bridge, indicates that double bond is an efficient unit to enlarge the adsorption range. **FWD2** and **FWD3** showed a significantly higher molar extinction coefficient (ϵ) compared to that of **FWD1**, indicating improved light harvesting capabilities for **FWD2** and **FWD3** due to their better coplanarity, which always results in a wider adsorption range and higher molar extinction coefficient [28].

In general, hypsochromic shift would be observed after attaching dyes on TiO_2 films due to the *H*-aggregation (plane-to-plane π stacking) of the dyes on semiconductor surface [29]. The absorption maxima for **FWDs** on 2 μm TiO_2 transparent films were 414, 424 and 413 nm, respectively. The data were almost same with that in EtOH and indicated that no *H*-aggregations for **FWDs** on TiO_2 films were observed. The reason for this result should be the pyramidal structure of the triphenylamine moiety that avoid the issue of plane-to-plane π -stacking.

2.3 Electrochemical properties

The Cyclic voltammetry was performed to investigate the electrochemical properties of **FWDs** and also the possibilities of electron injections from the excited dyes into TiO_2 conduction band and dye regenerations by redox electrolytes [26]. The cyclic voltammograms are represented in Fig. 2 and the relevant data are summarized in Table 1.

Fig. 2. CV plots of **FWDs**.

Fig. 3. The energy band diagram of **FWDs**.

The first oxidation peak potentials (E_{ox}) (refers to the HOMO level) of **FWDs** were 1.30, 1.09 and 1.35 V, respectively. The results are summarized in energy band diagrams in Fig. 3. The values were more positive than the I_3/I^- redox potential value (0.4 V vs NHE), which guarantees efficient dye regeneration of the oxidized dyes by the electrolyte [30]. E_{ox} value of **FWD2** is significant lower compared with that of **FWD1** and **FWD3**, which could be attributed to its double bonds moiety. It suggests that **FWD2** can be easily excited to its higher energy level. Thus, **FWD2** can undergo the charge transfer easily and this might be part of the reason why **FWD2**-based DSSC exhibited the best photovoltaic performances.

The band gap energies (E_{0-0}) of **FWDs** were 2.46, 2.34 and 2.48 V, respectively, which were estimated from the onset wavelengths in the absorption spectra of the dyes in EtOH [31]. E_{red} (refers to the LUMO level) can be calculated from $E_{ox} - E_{0-0}$. The E_{red} of **FWDs** (-1.16, -1.25 and -1.13 V, respectively) were sufficiently more negative than the Fermi level of TiO_2 (-0.5 V vs NHE), providing the thermodynamic feasibility of electron injection from the excited dye molecules into the conduction band of the TiO_2 semiconductor [30]. These results clearly demonstrated that **FWDs** could be potentially efficient sensitizers to be used in DSSCs.

2.4 Theoretical calculation

To investigate the geometrical structures and electron distributions of **FWDs**, the geometries and energies of the dyes were optimized by density functional theory (DFT) calculations with the B3LYP exchange correlation functional under the 6-31G(d) basis set implemented in the Gaussian 09 program. The optimized structure and electron distribution of **FWDs** are shown in Fig. 4, with the isodensity surface values fixed at 0.02.

Fig. 4. The optimized structure and electron distribution of the HOMO and LUMO of **FWDs**.

According to the corresponding molecular orbital profiles, the HOMOs of these dyes uniformly distributed over the whole molecules, while the LUMOs delocalized over the electron

accepter parts. It means that the electrons can easily transfer from the electron donor part to the acceptor part and hence an efficient electron injection from the excited dyes into the acceptor group-connected TiO₂. In the optimized structures of **FWD1**, the two benzene rings of the biphenyl part could not be coplanar, which restricted the conjugation extent. For **FWD2** and **FWD3**, the two benzene rings of the diphenylethene and diphenylethyne parts were parallel, which would exhibit an extended conjugation range and hence the higher molar extinction coefficients. The smallest calculated band gap (LUMO-HOMO) of **FWD2** is well coincidence with the λ_{abs} of **FWD2** (Table 1). **FWD3** showed the smallest dipole moment ($\mu = 8.06$ Debye) compared with **FWD1** (8.38 Debye) and **FWD2** (8.31 Debye). The small dipole moment might be adverse to intramolecular charge transfer from donor to acceptor part resulting in the lowest power conversion efficiency for **FWD3**-based DSSC [27].

2.5 Photovoltaic properties

Fig. 5. *J-V* curves (a) and IPCE plots (b) of DSSCs based **FWDs**.

Table 2

Photovoltaic performances parameters and simulated EIS data of DSSCs based on **FWDs**.

Dye	$J_{sc}/\text{mA cm}^{-2}$	V_{oc}/V	FF	$\eta/\%$	$I/\text{mol cm}^{-2}$	τ_e/ms	$R_s/\Omega \text{ cm}^{-2}$	$R_{CE}/\Omega \text{ cm}^{-2}$	$R_{rec}/\Omega \text{ cm}^{-2}$
FWD1	10.04	0.77	0.73	5.65	1.74×10^{-7}	96.8	7.1	11.7	362.6
FWD2	10.91	0.75	0.74	6.04	2.17×10^{-7}	96.8	15.6	8.9	382.0
FWD3	9.12	0.78	0.73	5.19	1.95×10^{-7}	179.7	10.7	14.2	501.9
TC ^a	5.26	0.64	0.78	2.60	-	-	-	-	-

^a See ref. [26].

Fig. 5a shows the current density-voltage (*J-V*) curves of the DSSCs sensitized with **FWDs** under AM 1.5G irradiation (1 sun, 100 mW cm^{-2}), the cells were measured without mask in a 0.16 cm^2 working area. Their corresponding photoelectrochemical properties, namely short-circuit current

density (J_{sc}), open circuit voltage (V_{oc}), fill factor (FF) and power conversion efficiency (η) data are listed in Table 2. **FWD2**-based DSSC exhibited the highest short-circuit photocurrent density (J_{sc}) of 10.91 mA cm⁻² while the J_{sc} values for **FWD1**-based and **FWD3**-based DSSCs were 10.04 and 9.12 mA cm⁻², respectively. High open circuit voltage (V_{oc}) values were observed for these DSSCs (0.77 V for **FWD1**, 0.75 V for **FWD2** and 0.78 V for **FWD3**). As a result, excellent power conversion efficiencies (η) were achieved by **FWDs**-based DSSCs (5.65% for **FWD1**, 6.04% for **FWD2** and 5.19% for **FWD3**). The best power conversion efficiency for **FWD2**-based DSSC was mainly because of its highest short-circuit photocurrent density, which was attributed to the widest absorption spectrum for **FWD2** and also probably the highest dye loading amount (Γ) of **FWD2** on TiO₂ [32]. All of the DSSCs based on **FWDs** showed significant improved performances compared with that of **TC**. The results indicated that it is an effective way to get efficient dyes by introducing extra phenyl rings into donor moiety, especially adopting double bonds as the bridge.

The IPCE (Incident Photon-to-current Conversion Efficiency) spectra of the DSSCs exhibited response in the region of 300-600 nm and showed plateau nearly 80% in the range from 400 to 510 nm (Fig. 5b). The broadest IPCE response range of **FWD2**-based DSSC explained the highest J_{sc} value of it from the J - V measurement, which is consistent with the widest absorption spectrum of **FWD2**.

2.6 Electrochemical impedance spectroscopy

Electrochemical impedance spectroscopy (EIS) of the DSSCs in dark under an applied dc voltage equivalent to V_{oc} of the device were measured to further determine photovoltaic properties of **FWDs**. Nyquist plots and Bode phase plots of DSSCs based on **FWDs** and the equivalent circuit are shown in Fig. 6 and the relevant data are listed in Table 2.

Fig. 6. Nyquist plots (a) and Bode plots (b) of the DSSCs based on **FWDs** and the equivalent circuit (c).

The series resistance (R_s) values of these three cells ($7.1 \Omega \text{ cm}^{-2}$ for **FWD1**, $15.6 \Omega \text{ cm}^{-2}$ for **FWD2** and $10.7 \Omega \text{ cm}^{-2}$ for **FWD3**) are similar because of the same electrolyte and electrode in both materials and surface area [33]. The small charge values of transfer resistances at the interface of Pt/electrolyte (R_{CE}) ($11.7 \Omega \text{ cm}^{-2}$ for **FWD1**, $8.9 \Omega \text{ cm}^{-2}$ for **FWD2** and $14.2 \Omega \text{ cm}^{-2}$ for **FWD3**) represented the rapid reduction of I_3^- ions on Pt counter electrode [34]. The larger semicircle at lower frequencies indicates charge recombination resistance at the $\text{TiO}_2/\text{dye}/\text{electrolyte}$ (R_{rec}), which give information about the charge transfer at $\text{TiO}_2/\text{Dye}/\text{Electrolyte}$ interface. Large R_{rec} values of these three cells ($362.6 \Omega \text{ cm}^{-2}$ for **FWD1**, $382.0 \Omega \text{ cm}^{-2}$ for **FWD2** and $501.9 \Omega \text{ cm}^{-2}$ for **FWD3**) guaranteed high open circuit voltage [34]. The electron lifetime (τ_e) can be estimated according to $\tau_e = 1/2\pi f$ [35], while f is the peak frequency at lower frequency region in the Bode phase plots (1.6 Hz for **FWD1**, 1.6 Hz for **FWD2** and 0.9 Hz for **FWD3**) corresponds to the $\text{TiO}_2/\text{dye}/\text{electrolyte}$ interface. Typically, higher τ_e value would lead to a higher V_{oc} [36]. **FWD3** showed the highest τ_e (179.7 ms). As a result, the highest V_{oc} was observed for **FWD3**-based DSSC.

3 Experimental

3.1 Reagents and materials

All reagents obtained from commercial sources were used as received, unless otherwise noted. Toluene and diisopropylamine were distilled from CaH_2 before used. FTO conductive glasses (sheet resistance $7 \Omega/\text{sq}$, 2.2 mm thick) were used for DSSCs fabrication. Electrolyte for DSSCs fabrication: LiI (0.1 M), I_2 (0.1 M), 4-tert-butylpyridine (1.0 M) and 1,2-dimethyl-3-propylimidazolium iodide (0.6 M) in acetonitrile.

3.2 Instruments and characterization

Melting points were measured on an X-4A apparatus. ^1H NMR and ^{13}C NMR spectra were recorded at room temperature on Bruker DRX300 or Bruker AVANCE III 500 instruments and calibrated with tetramethylsilane (TMS) as an internal reference. HRMS were recorded by Waters Q-TOF MicroTM. UV-Vis absorption spectra were recorded by THERMO FISHER EVOLUTION220 at room temperature. Cyclic voltammetry measurements of dyes were carried out with a Versa STAT3 electrochemical workstation in tetrahydrofuran (THF) (1.0×10^{-3} M) containing 0.1 M Bu_4NPF_6 as the supporting electrolyte, and a three-electrode system (glassy carbon as the working electrode, platinum wire as the counter electrode, and Ag/AgCl as reference electrode). Ferrocene was used as the external standard. The scan rate was 50 mV/s. The IPCE were measured by PECCELL PEC-S20 action spectrum measurement with monochromatic incident light under 100 mW cm^{-2} with bias light in DC mode (150 W xenon lamp). Current density-voltage measurements were carried out using simulated 1.5 AM sunlight with an output power of 100 mW cm^{-2} (PECELL-L15). Electrochemical impedance spectroscopy (EIS) were measured by Zahner Zennium Impedance Analyzer in the frequency range of 10^{-1} - 10^5 Hz under 1 sun bias illumination under an open-circuit condition. The amount of dye load was measured by desorbing the dye from the films with 0.1 M tetrabutylammonium hydroxide in THF/ H_2O (1:1) and measuring the corresponding UV-vis spectrum.

3.3 Synthesis of sensitizers

All reactions were carried out under an atmosphere of nitrogen unless otherwise noted. 4-(bis(4-iodophenyl)amino)benzaldehyde was synthesized according to the literature [27].

3.3.1 4-(di([1,1'-biphenyl]-4-yl)amino)benzaldehyde (**I**)

To a round-bottom flask were added 4-(bis(4-iodophenyl)amino)benzaldehyde (1470 mg, 2.80 mmol), $\text{Pd}(\text{PPh}_3)_4$ (325 mg, 0.28 mmol), K_2CO_3 (3100 mg, 22.4 mmol) and phenylboronic acid

(821 mg, 6.72 mmol), 1,4-dioxane (32 mL) and water (8 mL), and the mixture was stirred at 80°C overnight. After cooling, the reaction mixture was extracted with dichloromethane. The organic layer was dried over anhydrous Na₂SO₄. After filtration, the solvents were removed by rotary evaporation. The crude product was chromatographed on silica gel eluting with petroleum ether and dichloromethane (1:1) to afford 1010 mg (84.8%) of **1** as a yellow solid.

M.p.: 101.7-102.7°C. ¹H NMR (300 MHz, CDCl₃) δ: 7.14 (d, *J* = 8.7 Hz, 2H), 7.27 (d, *J* = 8.7 Hz, 4H), 7.35 (t, *J* = 7.5 Hz, 2H), 7.45 (t, *J* = 7.4 Hz, 4H), 7.57-7.61 (m, 8H), 7.73 (d, *J* = 8.7 Hz, 2H), 9.84(s, 1H).

3.3.2 4-(bis(4-styrylphenyl)amino)benzaldehyde (**2**)

To a round-bottom flask were added 4-(bis(4-iodophenyl)amino)benzaldehyde (1470 mg, 2.80 mmol), Pd(PPh₃)₄ (325 mg, 0.28 mmol), K₂CO₃ (3100 mg, 22.4 mmol) and styrene (1170 mg, 6.72 mmol), 1,4-dioxane (32 mL) and water (8 mL), and the mixture was stirred at 90°C overnight. After cooling, the reaction mixture was extracted with dichloromethane. The organic layer was dried over anhydrous Na₂SO₄. After filtration, the solvents were removed by rotary evaporation. The crude product was chromatographed on silica gel eluting with petroleum ether and dichloromethane (1:1) to afford 1220 mg (91.2%) of **2** as a yellow solid.

M.p.: 114.4-115.2°C. ¹H NMR (500 MHz, CDCl₃) δ: 7.08 (s, 2H), 7.09 (s, 2H), 7.12 (d, *J* = 8.5 Hz, 2H), 7.16 (d, *J* = 8.5 Hz, 4H), 7.28 (d, *J* = 8.5 Hz, 2H), 7.37 (t, *J* = 7.5 Hz, 4H), 7.48-7.52 (m, 8H), 7.72 (d, *J* = 8.5 Hz, 2H), 9.84(s, 1H).

3.3.3 4-(bis(4-(phenylethynyl)phenyl)amino)benzaldehyde (**3**)

To a round-bottom flask were added 4-(bis(4-iodophenyl)amino)benzaldehyde (1470 mg, 2.80 mmol), Pd(PPh₃)₂Cl₂ (196 mg, 0.28 mmol), CuI (53 mg, 0.10 mmol) and phenylacetylene (600 mg, 6.16 mmol), toluene (40 mL) and diisopropylamine (5 mL), and the mixture was stirred at room

temperature overnight. Then the reaction mixture was extracted with dichloromethane. The organic layer was dried over anhydrous Na_2SO_4 . After filtration, the solvents were removed by rotary evaporation. The crude product was chromatographed on silica gel eluting with petroleum ether and dichloromethane (1:1) to afford 1250 mg (94.0%) of **3** as a yellow solid.

M.p.: 77.9-78.8°C. ^1H NMR (300 MHz, CDCl_3) δ : 7.11-7.15(m, 6H), 7.34-7.36 (m, 6H), 7.48-7.54 (m, 8H), 7.74 (d, $J = 9.0$ Hz, 2H), 9.86(s, 1H).

3.3.4 2-cyano-3-(4-(di([1,1'-biphenyl]-4-yl)amino)phenyl)acrylic acid (**FWD1**)

To a round-bottom flask were added **1** (766 mg, 1.80 mmol), $\text{CH}_3\text{COONH}_4$ (333 mg, 4.32 mmol), cyanoacetic acid (291 mg, 3.42 mmol) and acetic acid (40 mL) was heated to reflux for 5 h. After cooling, the mixture was poured into 200 mL of water. After filtration, the residue was recrystallized with CH_2Cl_2 to afford 476 mg (53.8%) of **FWD1** as a red solid.

M.p.: 152.0-152.9°C. ^1H NMR (300 MHz, DMSO) δ : 7.03 (d, $J = 8.7$ Hz, 2H), 7.31 (d, $J = 8.4$ Hz, 4H), 7.36 (d, $J = 7.2$ Hz, 2H), 7.47 (t, $J = 7.7$ Hz, 4H), 7.67-7.75 (m, 8H), 7.97 (d, $J = 8.7$ Hz, 2H), 8.17(s, 1H). ^{13}C NMR (125 MHz, DMSO) δ : 99.42, 117.28, 119.55, 123.93, 126.36, 126.51, 127.47, 128.21, 128.02, 132.82, 136.03, 139.33, 144.70, 151.22, 152.85, 164.46. HRMS (ESI) m/z : calcd for (M-H) $^-$ $\text{C}_{34}\text{H}_{23}\text{N}_2\text{O}_2$: 491.1765, found: 491.1768.

3.3.5 3-(4-(bis(4-styrylphenyl)amino)phenyl)-2-cyanoacrylic acid (**FWD2**)

To a round-bottom flask were added **2** (860 mg, 1.80 mmol), $\text{CH}_3\text{COONH}_4$ (333 mg, 4.32 mmol), cyanoacetic acid (291 mg, 3.42 mmol) and acetic acid (40 mL) was heated to reflux for 5 h. After cooling, the mixture was poured into 200 mL of water. After filtration, the residue was recrystallized with CH_2Cl_2 to afford 411 mg (42.0%) of **FWD2** as a red solid.

M.p.: 154.0-155.1°C. ^1H NMR (300 MHz, DMSO) δ : 7.01 (d, $J = 8.7$ Hz, 2H), 7.18-7.31 (m, 10H), 7.38 (t, $J = 7.5$ Hz, 4H), 7.59-7.67 (m, 8H), 7.96 (d, $J = 9.0$ Hz, 2H), 8.17 (s, 1H) 13.62 (br, 1H).

^{13}C NMR (125 MHz, DMSO) δ : 98.57, 117.07, 119.70, 123.85, 126.04, 126.54, 127.63, 128.06, 128.39, 128.78, 132.93, 134.18, 137.09, 144.53, 151.22, 153.26, 164.18. HRMS (ESI⁻) m/z : calcd for (M-H)⁻ C₃₈H₂₇N₂O₂: 543.2078, found: 543.2084.

3.3.6 3-(4-(bis(4-(phenylethynyl)phenyl)amino)phenyl)-2-cyanoacrylic acid (**FWD3**)

To a round-bottom flask were added **3** (1040 mg, 2.20 mmol), CH₃COONH₄ (407 mg, 5.28 mmol), cyanoacetic acid (356 mg, 4.18 mmol) and acetic acid (48 mL) was heated to reflux for 5 h. After cooling, the mixture was poured into 200 mL of water. After filtration, the residue chromatographed on silica gel eluting with dichloromethane and methanol (30:1 to 10:1) to afford 610 mg (51.3%) of **FWD3** as a red solid.

M.p.: 152.3-153.0°C. ^1H NMR (500 MHz, DMSO) δ : 7.10-7.14 (m, 6H), 7.42-7.43 (m, 6H), 7.54-7.55 (m, 8H), 7.89 (d, $J = 8.5$ Hz, 2H), 7.98 (s, 1H). ^{13}C NMR (125 MHz, DMSO) δ : 89.13, 89.43, 118.12, 122.22, 122.40, 125.04, 126.50, 128.78, 131.33, 132.00, 133.05, 145.83, 149.38, 150.04, 164.00. HRMS (ESI⁻) m/z : calcd for (M-H)⁻ C₃₈H₂₃N₂O₂: 539.1765, found: 539.1772.

3.4 Fabrication of DSSCs

Working electrodes (4*4 mm, 0.16 cm²) with a 15 μm thick transparent TiO₂ (20 nm) layer and a 5 μm thick TiO₂ (200 and 400 nm) scattering layer were heated at 80 °C for 30 min before using. The electrodes were immersed in the dye solutions (0.3 mM in CHCl₃) for 12 h. Then the electrodes were flushed with EtOH and dried in air for use. Liquid electrolytes, which consists of LiI (0.1 M), I₂ (0.1 M), 4-tert-butylpyridine (1.0 M) and 1,2-dimethyl-3-propylimidazolium iodide (0.6 M) in acetonitrile, was added dropwise onto the electrodes. The counter electrodes and working electrodes were sandwiched to be dye-sensitized solar cells without mask for the measurements.

4 Conclusions

In summary, three small molecule (molecular weight is around 500 Da) organic dyes (**FWD1**, **FWD2** and **FWD3**) were synthesized by introducing two extra phenyl units to TPA units of TC bridged with single bonds, double bonds or triple bonds, respectively. The optical and electrochemical properties, theoretical studies and photovoltaic parameters of DSSCs based on these dyes were systematically investigated. The DSSCs based on **FWDs** exhibited well performances: the short-circuit current density (J_{sc}) of 10.04, 10.91 and 9.12 mA cm⁻², respectively; the open circuit voltage (V_{oc}) of 0.77, 0.75 and 0.78 V, respectively; the power conversion efficiency (η) of 5.65%, 6.04% and 5.19%, respectively. Two extra phenyl units attached via double or triple bonds increase the planar nature of these molecules, increasing the loading amount, which ultimately can correlate into the received efficiency. The results indicated that it is an effective way to get efficient dyes by introducing extra phenyl rings into donor moiety, especially adopting double bonds as the bridge. Finally, efficient DSSCs were achieved by using small molecule TPA-type dyes **FWD1**, **FWD2** and **FWD3** as the sensitizers.

Acknowledgment

This work was supported by the Natural Science Foundation of Jiangsu Province (BK20140780).

Appendix A. Supplementary data

Supplementary data associated with this article can be found, in the online version, at <http://XXXXXXXXXXXXXXXX>.

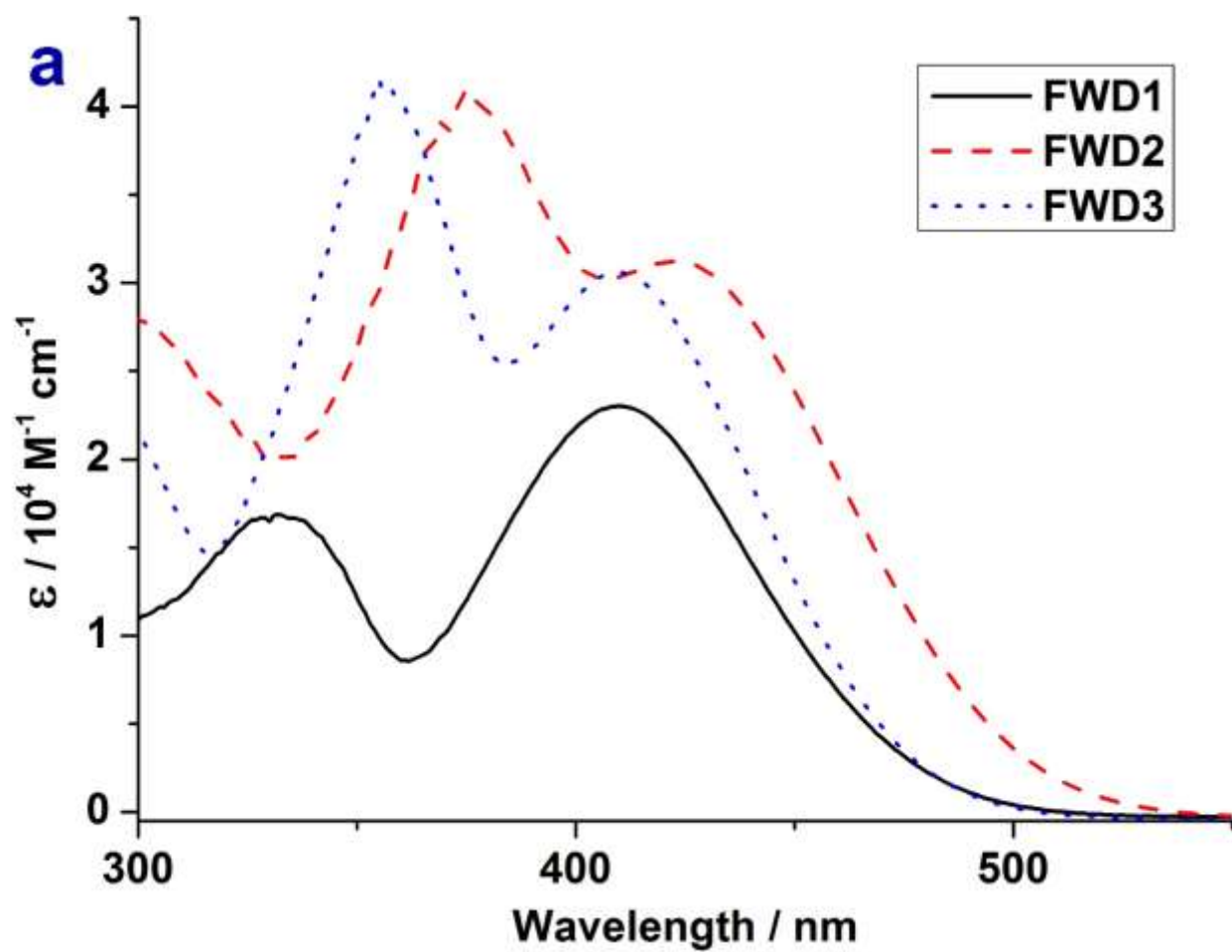
References

- [1] B. O'Regan, M. Grätzel, *Nature*, 353 (1991) 737-740.
- [2] M. Grätzel, *Accounts Chem Res*, 42 (2009) 1788-1798.
- [3] B. Pashaei, H. Shahroosvand, M. Graetzel, M.K. Nazeeruddin, *Chem Rev*, 116 (2016) 9485-9564.
- [4] J. Albero, P. Atienzar, A. Corma, H. Garcia, *Chem Rec*, 15 (2015) 803-828.
- [5] S. Chaurasia, C.J. Liang, Y.S. Yen, J.T. Lin, *J Mater Chem C*, 3 (2015) 9765-9780.
- [6] B. Cecconi, N. Manfredi, T. Montini, P. Fornasiero, A. Abbotto, *Eur J Org Chem*, (2016) 5194-5215.
- [7] G. Copley, D. Hwang, D. Kim, A. Osuka, *Angew Chem Int Edit*, 55 (2016) 10287-10291.

- [8] J.B. Yang, P. Ganesan, J. Teuscher, T. Moehl, Y.J. Kim, C.Y. Yi, P. Comte, K. Pei, T.W. Holcombe, M.K. Nazeeruddin, J.L. Hua, S.M. Zakeeruddin, H. Tian, M. Gratzel, *J Am Chem Soc*, 136 (2014) 5722-5730.
- [9] J.K. Fang, T. Sun, Y. Tian, Y. Zhang, C. Jin, Z. Xu, Y. Fang, X. Hu, H. Wang, *Mater. Chem. Phys.* 195 (2017) 1-9.
- [10] Z.F. Wu, X. Li, J. Li, H. Agren, J.L. Hua, H. Tian, *J Mater Chem A*, 3 (2015) 14325-14333.
- [11] J.Y. Wang, K. Liu, L.C. Ma, X.W. Zhan, *Chem Rev*, 116 (2016) 14675-14725.
- [12] J.Y. Mao, X.Y. Zhang, S.H. Liu, Z.J. Shen, X. Li, W.J. Wu, P.T. Chou, J.L. Hua, *Electrochim Acta*, 179 (2015) 179-186.
- [13] X. Yang, S. Kajiyama, J.K. Fang, F. Xu, Y. Uemura, N. Koumura, K. Hara, A. Orita, J. Otera, *B Chem Soc Jpn*, 85 (2012) 687-697.
- [14] M. Wielopolski, J.H. Kim, Y.S. Jung, Y.J. Yu, K.Y. Kay, T.W. Holcombe, S.M. Zakeeruddin, M. Gratzel, J.E. Moser, *J Phys Chem C*, 117 (2013) 13805-13815.
- [15] A. Mahmood, *Sol Energy*, 123 (2016) 127-144.
- [16] Y.H. Chiu, M. Shibahara, R.Y. Huang, M. Watanabe, Z.S. Wang, Y.J. Hsiao, B.F. Chang, T.H. Chiang, Y.J. Chang, *Dyes Pigments*, 136 (2017) 761-772.
- [17] T.N. Duan, K. Fan, T.Y. Peng, C. Zhong, Y. He, X.G. Chen, *Synthetic Met*, 211 (2016) 19-24.
- [18] K. Kakiage, Y. Aoyama, T. Yano, T. Otsuka, T. Kyomen, M. Unno, M. Hanaya, *Chem Commun*, 50 (2014) 6379-6381.
- [19] Z.Y. Yao, H. Wu, Y. Li, J.T. Wang, J. Zhang, M. Zhang, Y.C. Guo, P. Wang, *Energ Environ Sci*, 8 (2015) 3192-3197.
- [20] B. Liu, W.J. Wu, X.Y. Li, L. Li, S.F. Guo, X.R. Wei, W.H. Zhu, Q.B. Liu, *Phys Chem Chem Phys*, 13 (2011) 8985-8992.
- [21] J.X. Cheng, Z.S. Huang, L.Y. Wang, D.R. Cao, *Dyes Pigments*, 131 (2016) 134-144.
- [22] Y.Q. Wang, B. Chen, W.J. Wu, X. Li, W.H. Zhu, H. Tian, Y.S. Xie, *Angew Chem Int Edit*, 53 (2014) 10779-10783.
- [23] C. Teng, X.C. Yang, C. Yang, S.F. Li, M. Cheng, A. Hagfeldt, L.C. Sun, *J Phys Chem C*, 114 (2010) 9101-9110.
- [24] H.Y. Li, M.M. Fang, Y.Q. Hou, R.L. Tang, Y.Z. Yang, C. Zhong, Q.Q. Li, Z. Li, *Acs Appl Mater Inter*, 8 (2016) 12134-12140.
- [25] J.K. Fang, X. Yu, X. Yang, W.F. Li, D.L. An, *Chinese J Org Chem*, 32 (2012) 1261-1269.
- [26] C. Teng, X.C. Yang, C. Yang, H.N. Tian, S.F. Li, X.N. Wang, A. Hagfeldt, L.C. Sun, *J Phys Chem C*, 114 (2010) 11305-11313.
- [27] R. Misra, R. Maragani, D. Arora, A. Sharma, G.D. Sharma, *Dyes Pigments*, 126 (2016) 38-45.
- [28] J.-K. Fang, T. Sun, Y. Fang, Z. Xu, H. Zou, Y. Liu, F. Ge, *J Chem Res*, 39 (2015) 487-491.
- [29] K.R. Mulhern, A. Orchard, D.F. Watson, M.R. Detty, *Langmuir*, 28 (2012) 7071-7082.
- [30] R.G.W. Jinadasa, B.H. Li, B. Schmitz, S. Kumar, Y. Hu, L. Kerr, H. Wang, *Chemsuschem*, 9 (2016) 2239-2249.
- [31] D. Kumar, K.R.J. Thomas, C.P. Lee, K.C. Ho, *J Org Chem*, 79 (2014) 3159-3172.
- [32] B. Nagarajan, S. Kushwaha, R. Elumalai, S. Mandal, K. Ramanujam, D. Raghavachari, *J Mater Chem A*, 5 (2017) 10289-10300.
- [33] Y. Liu, J. He, L. Han, J.R. Gao, *J Photoch Photobio A*, 332 (2017) 283-292.
- [34] K. Rajavelu, P. Rajakumar, M. Sudip, R. Kothandaraman, *New J Chem*, 40 (2016) 10246-10258.
- [35] X. Qian, X.Y. Wang, L. Shao, H.M. Li, R.C. Yan, L.X. Hou, *J Power Sources*, 326 (2016) 129-136.
- [36] Y.J. Chang, Y.J. Wu, P.T. Chou, M. Watanabe, T.J. Chow, *Thin Solid Films*, 558 (2014) 330-336.

Figure captions

- Fig. 1.** UV-Vis absorption spectra of **FWDs** in EtOH solutions (a) and adsorbed on TiO₂ films (b).
- Fig. 2.** CV plots of **FWDs**.
- Fig. 3.** The energy band diagram of **FWDs**.
- Fig. 4.** The optimized structure and electron distribution of the HOMO and LUMO of **FWDs**.
- Fig. 5.** *J-V* curves (a) and IPCE plots (b) of DSSCs based **FWDs**.
- Fig. 6.** Nyquist plots (a) and Bode plots (b) of the DSSCs based on **FWDs** and the equivalent circuit (c).



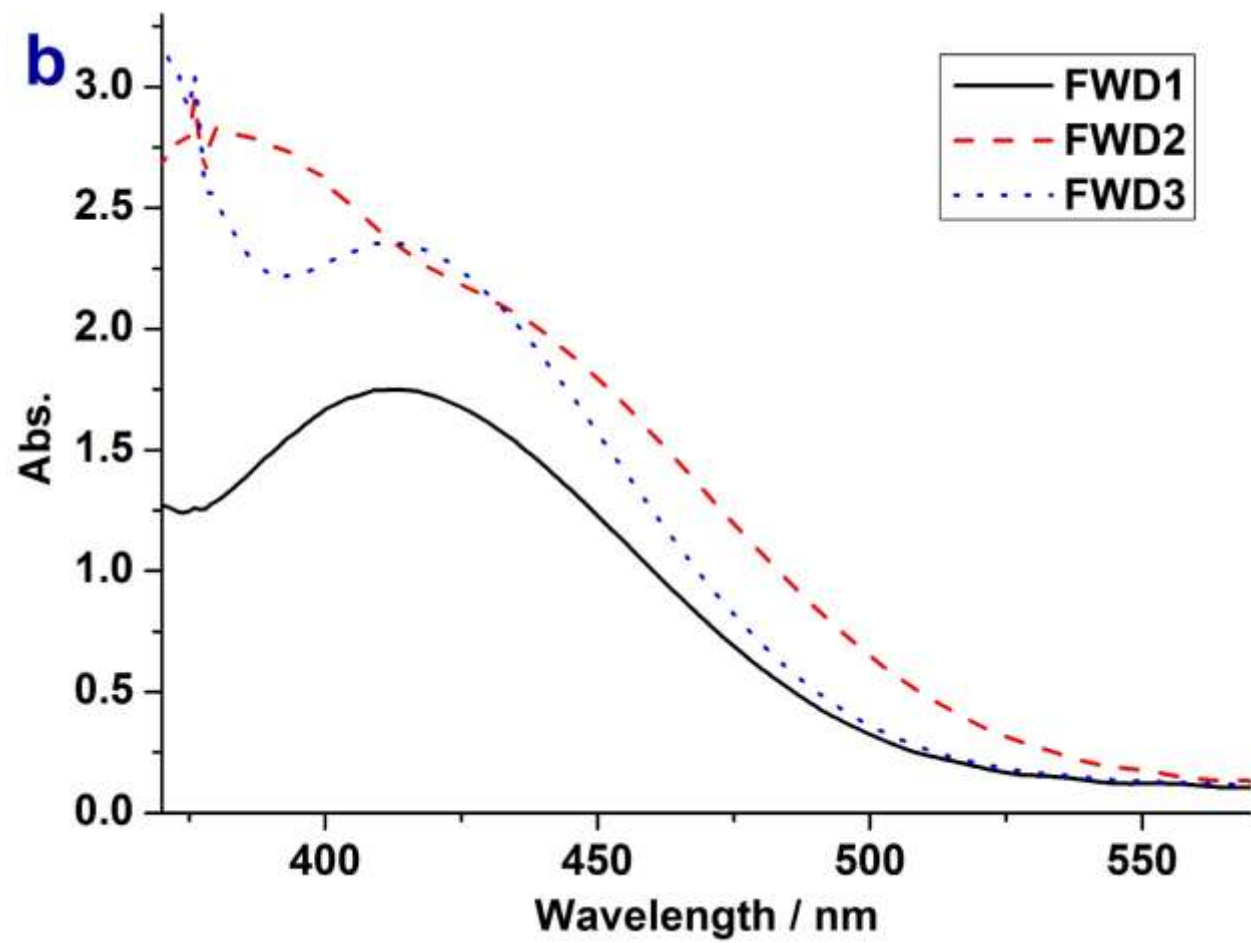


Fig 1

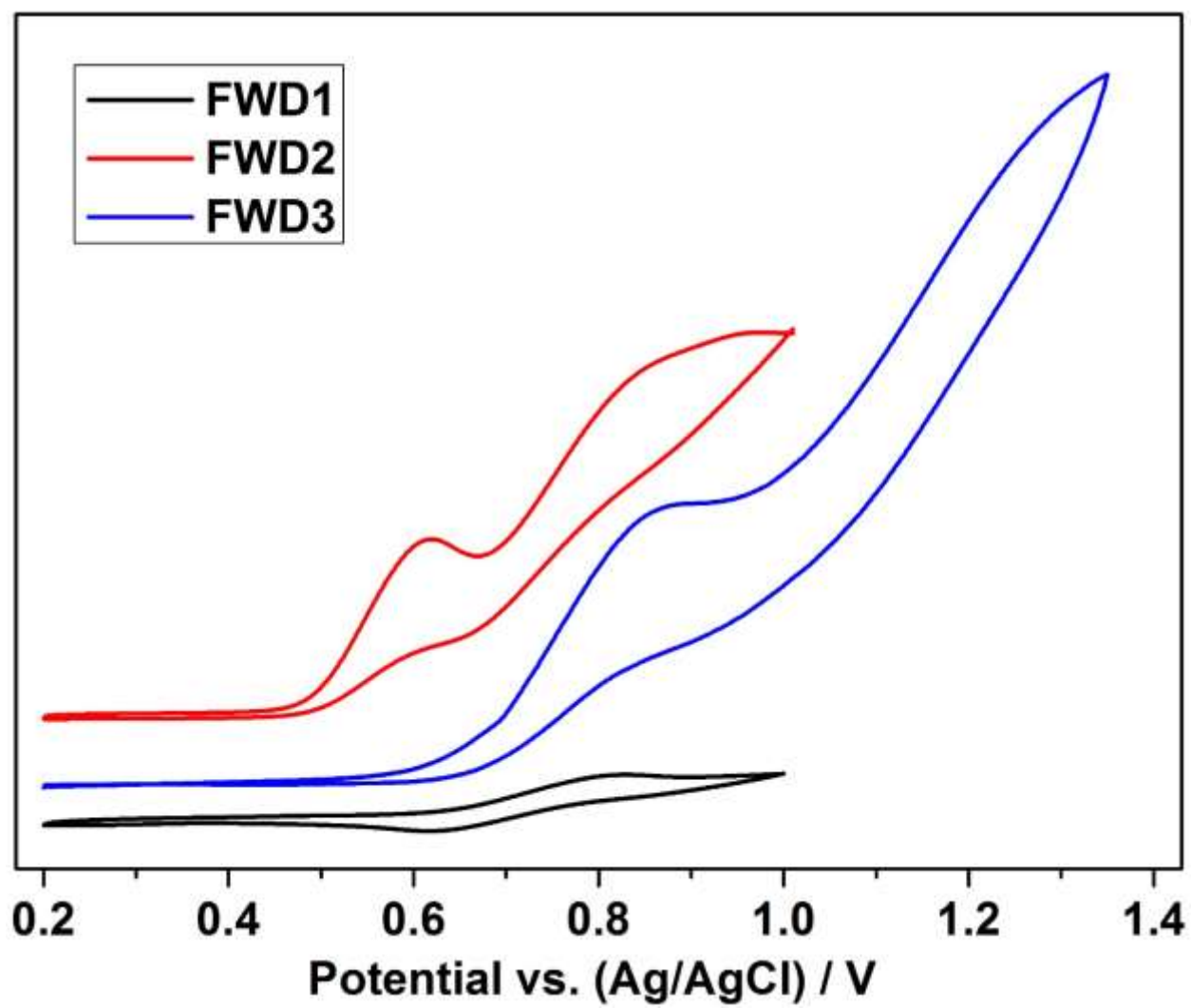


Fig 2

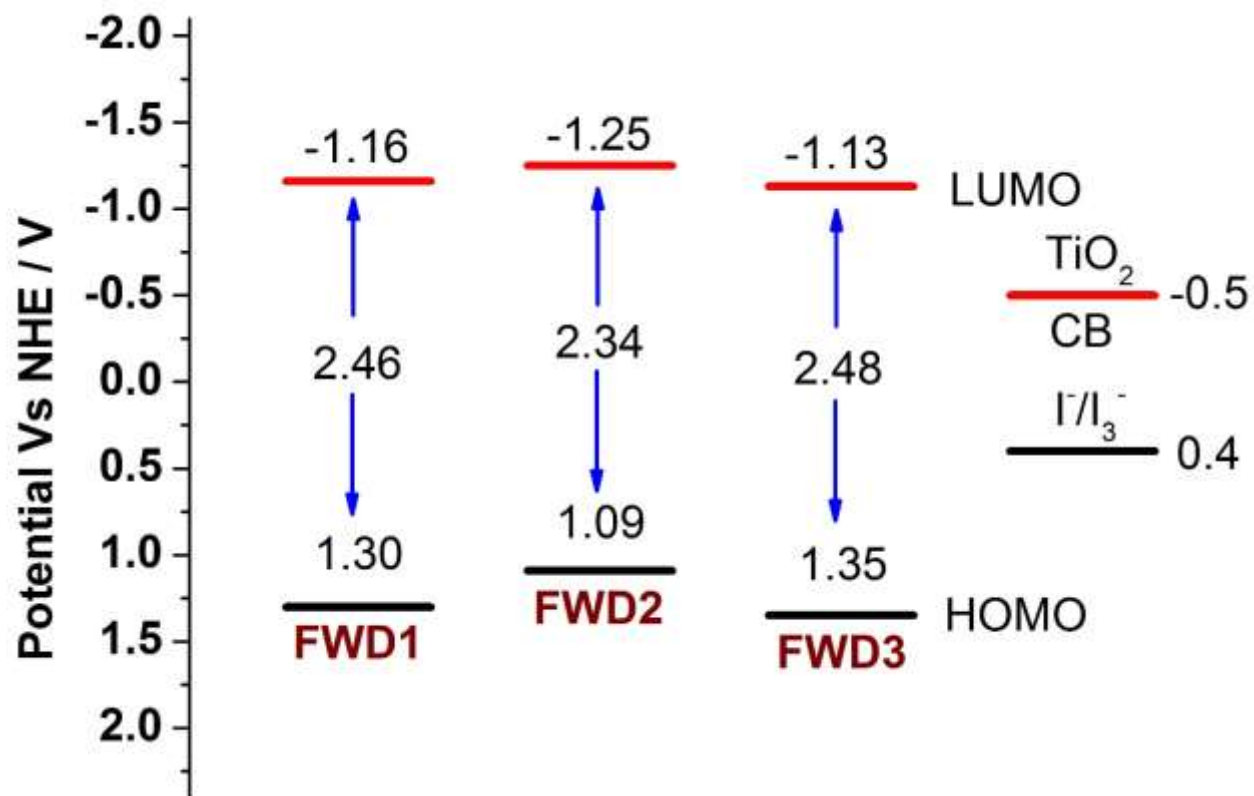


Fig 3

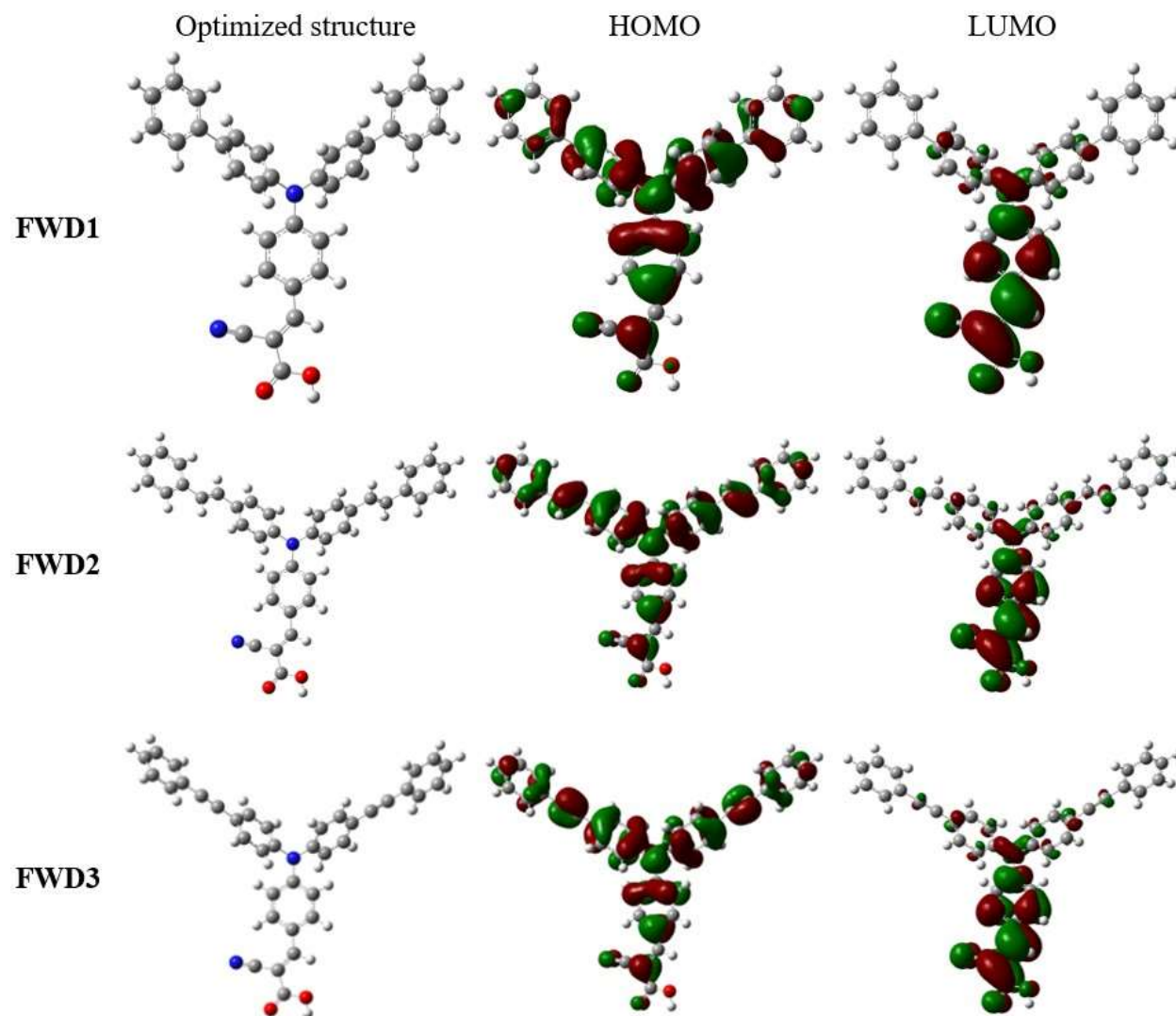
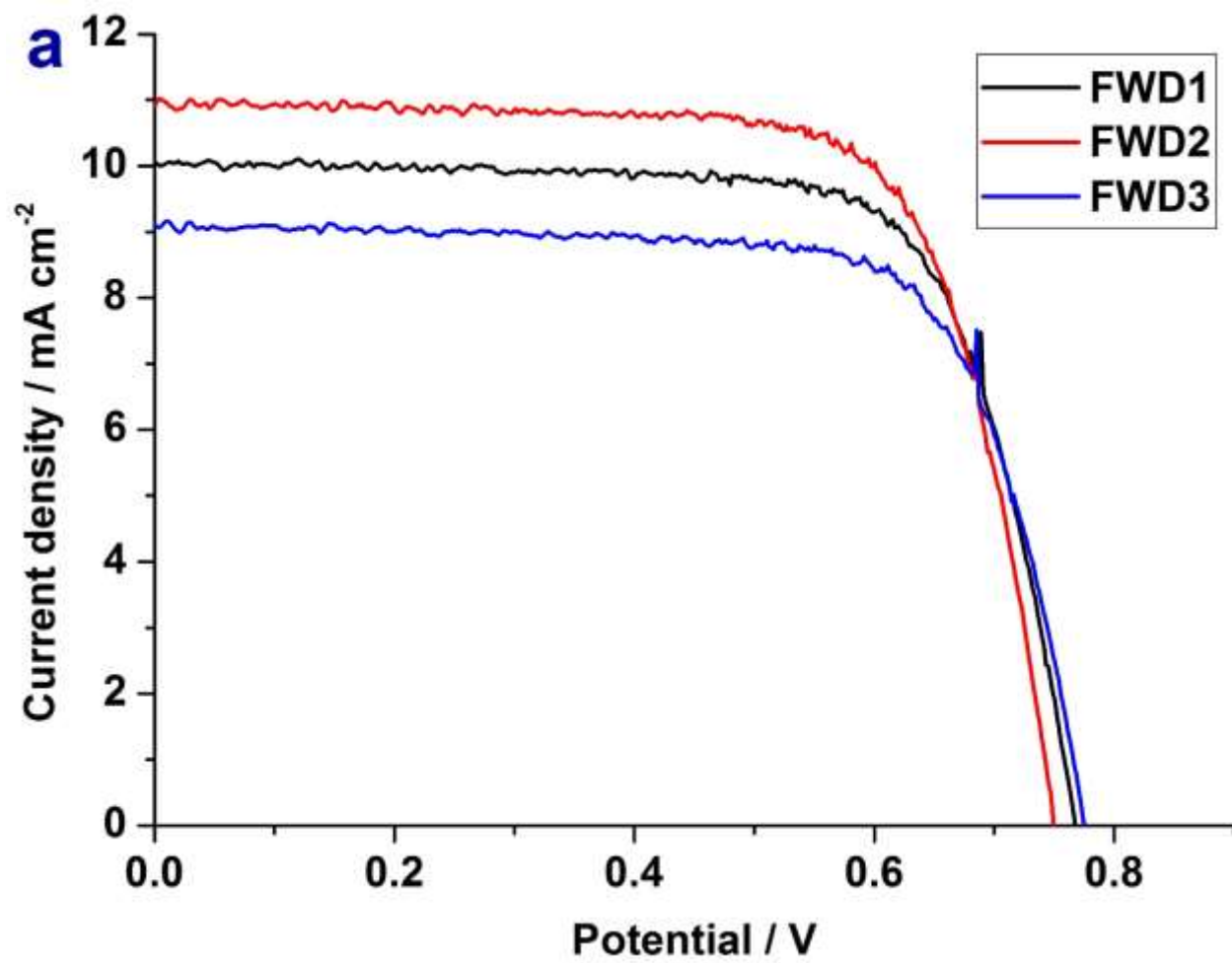


Fig 4



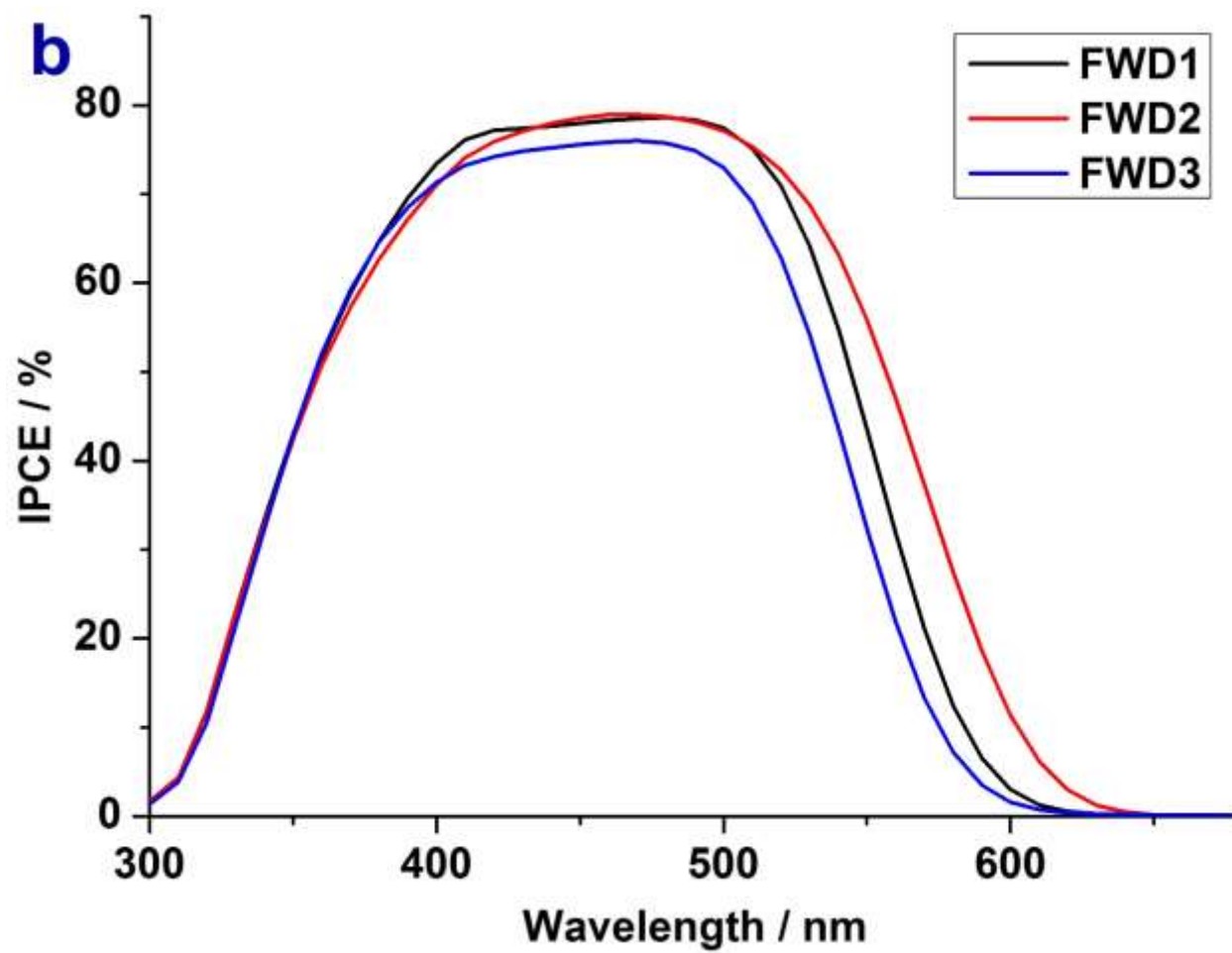
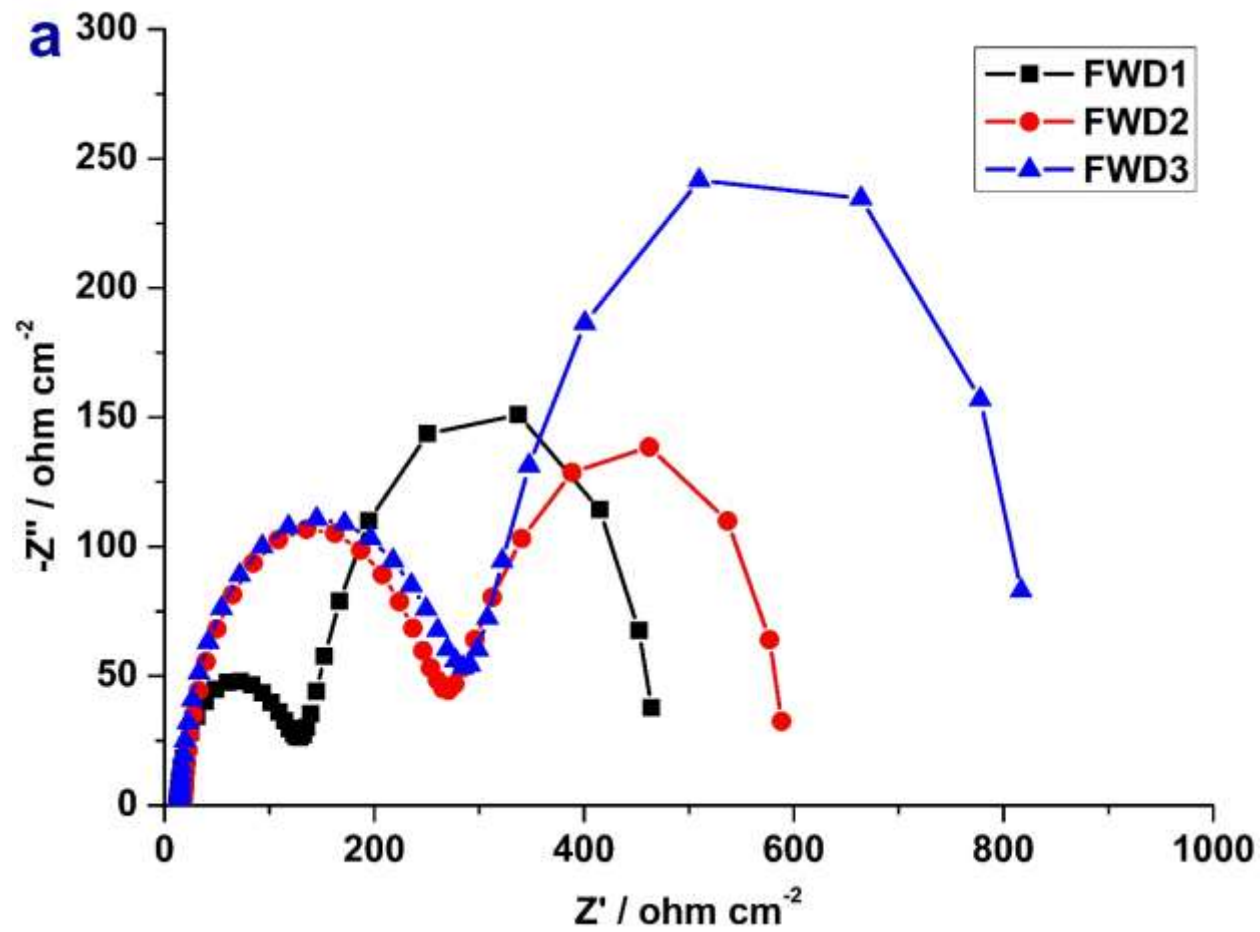
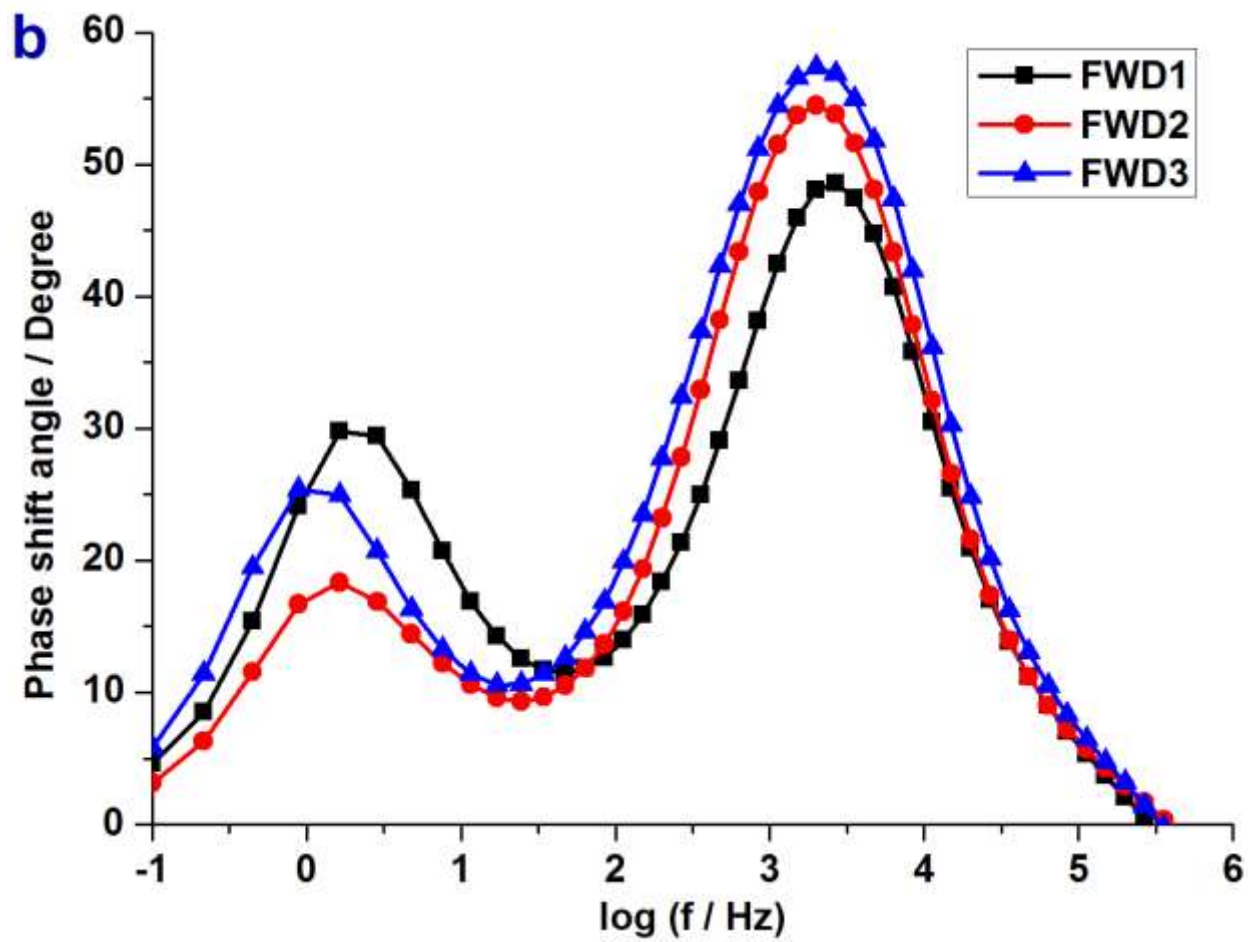


Fig 5





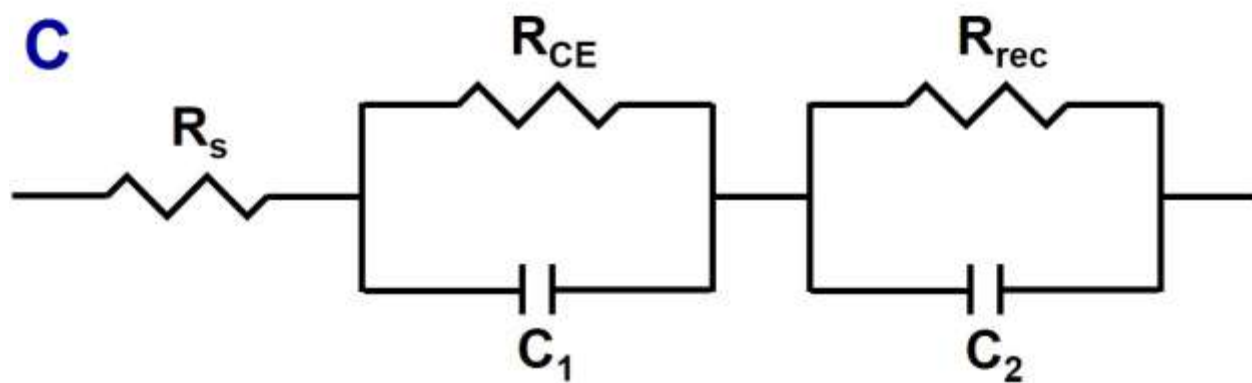


Fig 6